Koland, J. K., & Hammes, G. G. (1986) *J. Biol. Chem. 261*, 12428–12434.
Lacapere, J.-J., & Guillain, F. (1990) *J. Biol. Chem. 265*, 8583–8589.
Marquardt, D. W. (1963) *J. Soc. Ind. Appl. Math. 11*, 431.
Moczydlowski, E. G., & Fortes, P. A. G. (1981) *J. Biol. Chem. 256*, 2357–2366.
Moulton, M. P., Sabbadini, R. A., Norton, K. C., & Dahms, A. S. (1986) *J. Biol. Chem. 261* 12244–12251.
Murphy, A. J. (1990) *FEBS Lett. 263*, 175–177.
Pedersen, P. L, & Carafoli, E. (1987) *Trends Biochem. Sci. 12*, 146–150.
Pickart, C. M., & Jencks, W. P. (1982) *J. Biol. Chem. 257*, 5319–5322.
Pickart, C. M., & Jencks, W. P. (1984) *J. Biol. Chem. 259*, 1629–1643.
Post, R. L., Hegvary, C., & Kume, S. (1972) *J. Biol. Chem. 247*, 6530–6540.
Richards, D. E., Rega, A. F., & Garrahan, P. J. (1978) *Biochim. Biophys. Acta 511*, 194–201.
Ross, D. C., & McIntosh, D. B. (1987) *J. Biol. Chem. 262*, 12977–12983.
Schuster, S. M., Ebel, R. E., & Lardy, M. A. (1975) *J. Biol. Chem. 250*, 7848–7853.
Seebregts, C. J., & McIntosh D. B. (1989) *J. Biol. Chem. 264*, 2043–2052.
Stieger, J., & Luterbacher, S. (1981) *Biochim. Biophys. Acta 641*, 270–275.
Wallmark, B., Stewart, H. B., Rabon, E., Saccomani, G., & Sachs, G. (1980) *J. Biol. Chem. 255*, 5313–5319.
Yamamoto, T., & Tonomura, Y. (1967) *J. Biochem. (Tokyo) 62*, 558–575.

Conformation of $NADP^+$ Bound to a Type II Dihydrofolate Reductase†

Rui M. M. Brito,‡ Frederick B. Rudolph,‡ and Paul R. Rosevear*
Department of Biochemistry, Rice University, Houston, Texas 77005, and Department of Biochemistry and Molecular Biology, University of Texas Medical School at Houston, Houston, Texas 77225
Received September 10, 1990; Revised Manuscript Received November 6, 1990

ABSTRACT: Type II dihydrofolate reductases (DHFRs) encoded by the R67 and R388 plasmids are sequence and structurally different from known chromosomal DHFRs. These plasmid-derived DHFRs are responsible for confering trimethoprim resistance to the host strain. A derivative of R388 DHFR, RBG200, has been cloned and its physical properties have been characterized. This enzyme has been shown to transfer the *pro-R* hydrogen of NADPH to its substrate, dihydrofolate, making it a member of the A-stereospecific class of dehydrogenases [Brito, R. M. M., Reddick, R., Bennett, G. N., Rudolph, F. B., & Rosevear, P. R. (1990) *Biochemistry 29*, 9825]. Two distinct binary RBG200·$NADP^+$ complexes were detected. Addition of $NADP^+$ to RBG200 DHFR results in formation of an initial binary complex, conformation I, which slowly interconverts to a second more stable binary complex, conformation II. The binding of $NADP^+$ to RBG200 DHFR in the second binary complex was found to be weak, $K_D = 1.9 \pm 0.4$ mM. Transferred NOEs were used to determine the conformation of $NADP^+$ bound to RBG200 DHFR. The initial slope of the NOE buildup curves, measured from the intensity of the cross-peaks as a function of the mixing time in NOESY spectra, allowed interproton distances on enzyme-bound $NADP^+$ to be estimated. The experimentally measured distances were used to define upper and lower bound distance constraints between proton pairs in distance geometry calculations. All $NADP^+$ structures consistent with the experimental distance bounds were found to have a syn conformation about the nicotinamide–ribose ($\chi = 94 \pm 26°$) and an anti conformation about the adenine–ribose ($\chi = -92 \pm 32°$) glycosidic bonds. The conformation of $NADP^+$ bound to RBG200 DHFR in the initial binary complex was qualitatively evaluated at 5 °C, to decrease the rate of interconversion to conformation II. The ratio of cross-peak intensities as well as the pattern of observed NOEs was only consistent with syn and anti conformations about the nicotinamide–ribose and adenine–ribose bonds, respectively, in the initial complex, conformation I. From the known stereochemistry of hydride transfer and the conformation of the enzyme-bound cofactor, a model is proposed for the orientation of cofactor and substrate at the active site of RBG200 DHFR. In this model, the NMNH moiety of NADPH is bound in a syn conformation with the pteridine portion of dihydrofolate located below the plane of the nicotinamide ring and rotated 180° with respect to dihydrofolate binding in chromosomal DHFRs.

Dihydrofolate reductase (DHFR; EC 1.5.1.3)[1] catalyzes a central reaction in one-carbon metabolism, the NADPH-dependent reduction of 7,8-dihydrofolate to 5,6,7,8-tetrahydrofolate. Chromosomal DHFRs are the target for a number of antifolate agents such as trimethoprim and methotrexate, which function by depleting the metabolic pool of one-carbon units necessary for normal cellular function. Type II DHFRs

† This work was supported by National Institutes of Health Grant GM 41232 to P.R.R., National Cancer Institute Grant 14030 to F.B.R., and grants from the Robert A. Welch Foundation, C-1041 and AU-1025 to F.B.R. and P.R.R., respectively.
* Author to whom correspondence should be addressed at the University of Texas Medical School at Houston.
‡ Rice University.

[1] Abbreviations: DHFR, dihydrofolate reductase; TMP, trimethoprim; MTX, methotrexate; DHF, 7,8-dihydrofolate; EDTA, ethylenediaminetetraacetic acid; DTT, 1,4-dithiothreitol; DSS, sodium 2,2-dimethyl-2-silapentane-5-sulfonate; DQCOSY, double quantum filtered two-dimensional correlated spectroscopy; NOESY, two-dimensional nuclear Overhauser enhancement spectroscopy; NOE, nuclear Overhauser effect; NMN, nicotinamide mononucleotide; AMN, adenine mononucleotide; TNOE, transferred nuclear Overhauser effect.

0006-2960/91/0430-1461$02.50/0

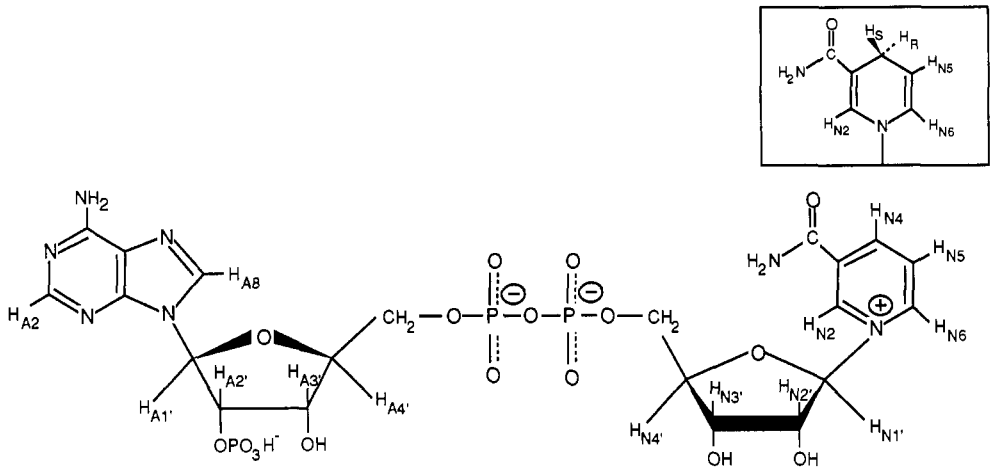

FIGURE 1: Numbering system for proton identification in $NADP^+$ and NADPH (insert). Protons from the AMN and NMN moieties of $NADP^+$ are labeled with A and N, respectively. $NADP^+$ is drawn with the adenosine in the anti conformation and the nicotinamide in the syn conformation. The *pro-R* and *pro-S* hydrogens of NADPH are labeled H_R and H_S, respectively.

encoded by the plasmids R67 and R388 were originally isolated from trimethoprim-resistant bacteria (Fleming et al., 1972; Aymes & Smith, 1974; Skold & Widh, 1974). Characterization of these plasmid-derived DHFRs showed them to have no sequence homology with known chromosomal DHFRs and to be insensitive to TMP, MTX, and other antifolate compounds (Pattishall et al., 1977; Zolg & Hänggi, 1981; Hitchings & Smith, 1980).

A derivative of R388 DHFR, RBG200, that has the sequence Thr-Thr-Ser-Arg-Thr-Leu at the carboxy terminus in addition to the 78 amino acids per subunit of the R388 DHFR has been cloned, purified to homogeneity, and characterized (Vermersch et al., 1986; Brito et al., 1990). The solubility and physical properties of this type II DHFR make it the ideal choice for studying the mode of substrate and inhibitor binding by this unique class of proteins. The native protein was found to be a tetramer with a pH optimum of 5.9, similar to that previously reported for other type II DHFRs (Brito et al., 1990; Amyes & Smith, 1976). Two distinct RBG200 DHFR·$NADP^+$ binary complexes have been detected by NMR (Brito et al., 1990). Addition of $NADP^+$ to the enzyme results in formation of an initial binary complex, conformation I, which slowly interconverts to a more stable binary complex, conformation II. The stereochemistry of hydride transfer was investigated by using [4(*S*)-^{2}H,4(*R*)-^{1}H]NADPH. RBG200 DHFR was found to transfer the *pro-R* hydrogen of NADPH to dihydrofolate (Brito et al., 1990). Chromosomal DHFRs have previously been shown to transfer the *pro-R* hydrogen of NADPH (Charlton et al., 1979). Thus, type II DHFRs have the same hydride-transfer stereochemistry as found for chromosomal DHFRs.

The conformation and arrangement of substrates bound to chromosomal DHFRs from a variety of sources has been extensively studied by NMR, using transferred NOEs, and X-ray crystallography (Kraut & Matthews, 1986; You, 1982; Matthews et al., 1979; Feeney et al., 1983). All chromosomal DHFRs studied to date, by using either TNOE measurements or crystallography, have been found to bind the coenzyme with an anti conformation about the nicotinamide–ribose glycosidic bond. Thus, chromosomal-derived DHFRs obey the general rule that enzymes which transfer the C4 *pro-R* hydrogen bind the coenzyme with an anti conformation about the nicotinamide–ribose glycosidic bond (You, 1985; Benner, 1982; Oppenheimer, 1986). A crystal structure for a dimeric form of type II R67 DHFR, without substrate or coenzyme bound, has been obtained and found to consist of a symmetrical dimer composed of two β-barrel monomers (Matthews et al., 1986). However, the native R67 enzyme was previously shown to be a tetramer composed of four identical subunits (Smith et al., 1979). From modeling studies, using the crystallographic structure of the dimer, it was suggested that NADPH binds along a lengthwise cleft between the subunits with an anti conformation about both the nicotinamide–ribose and adenine–ribose glycosidic bonds (Figure 1).

Transferred NOEs were used to determine the conformation of $NADP^+$ bound to RBG200 DHFR. The initial slope measured from the intensity of the cross-peaks in NOESY spectra as a function of the mixing time allowed interproton distances on enzyme-bound $NADP^+$ to be estimated. The experimentally measured internuclear distances were used to define upper and lower bound distance constraints between these proton pairs in a distance geometry algorithm. The distance geometry algorithm allows the conformational space available to the enzyme-bound cofactor to be objectively searched. All structures consistent with the experimental distance bounds were found to have a syn conformation about the nicotinamide–ribose ($\chi = 94 \pm 26°$) and an anti conformation about the adenine–ribose ($\chi = -92 \pm 32°$) glycosidic bonds of $NADP^+$. From the stereochemistry of hydride transfer and the conformation of the enzyme-bound cofactor, a model is proposed for the arrangement of substrates at the active site of RBG200 DHFR.

Methods

Materials. $NADP^+$ was purchased from Boehringer. NADPH, dihydrofolate, and Chelex-100 were purchased from Sigma. ^2H_2O was obtained from Cambridge Isotope Laboratories. DEAE-Sepharose fast flow was purchased from Pharmacia. [4-^{3}H]$NADP^+$ was prepared as previously described (Brito et al., 1990). All other chemicals were of the highest quality commercially available.

Protein Preparation. RBG200 DHFR was purified from *Escherichia coli* cells bearing the plasmid RBG200 as previously described (Brito et al., 1990). Purification consisted of cell lysis, streptomycin sulfate precipitation, ammonium sulfate precipitation, and DEAE-Sepharose chromatography. Dihydrofolate reductase activity was assayed as described by Smith and Burchall (1983) except the buffer used was 50 mM potassium phosphate, 1 mM EDTA, and 1 mM DTT at pH = 5.9 (Brito et al., 1990). One enzyme unit is the quantity of enzyme required to convert 1 μmol of NADPH and dihydrofolate to $NADP^+$ and tetrahydrofolate per minute based

on an absorption coefficient of 12300 L mol^{-1} cm^{-1} at 340 nm (Smith & Burchall, 1983). Specific activities for RBG200 DHFR were routinely 2.8 units/mg. No detectable loss in activity was observed after NMR experiments, which occasionally lasted up to 1 week.

Analysis of Binding Data by NMR. Titration of RBG200 DHFR with oxidized coenzyme while monitoring the line width of the HN2 resonance was used to determine the K_D for $NADP^+$ binding to the second of the RBG200 DHFR·$NADP^+$ complexes. Titrations were performed by addition of known aliquots of $NADP^+$ over the range 0.5–25 mM, to a solution of 0.4 mM RBG200 DHFR. After each addition of coenzyme, the sample was incubated to allow equilibrium between conformations I and II to be reached. Line widths of the HN2 resonance were measured at half peak height.

In conditions of fast exchange, the observed line width (LW_{obsd}) of a ligand resonance is given by

$$LW_{obsd} = f_L(LW_L) + f_{PL}(LW_{PL}) \quad (1)$$

where f_L and f_{PL} are the molar fractions and LW_L and LW_{PL} are the line widths of free and enzyme-bound ligands, respectively (Campbell & Dwek, 1984). Rearrangement of eq 1 permits LW_{obsd} to be expressed as a function of f_{PL}, LW_L, and LW_{PL} (eq 2). The dissociation constant, K_D, which

$$LW_{obsd} = LW_L + (LW_{PL} - LW_L)f_{PL} \quad (2)$$

quantitates the affinity of the ligand (L) for the protein (P), is given by

$$K_D = ([P_T - PL])([L_T] - [PL])/[PL] \quad (3)$$

where $[L_T]$ and $[P_T]$ are the total concentrations of ligand and noninteracting homogeneous binding sites, respectively. With eq 3 solved for [PL] and f_{PL} defined as $[PL]/[L_T]$, a quadratic expression for f_{PL} is obtained (eq 4). If eq 2 and 4 are combined, K_D can be determined from nonlinear least-squares analysis of plots of LW_{obsd} as a function of $[L_T]$.

$$f_{PL} = \{([L_T] + [P_T] + K_D) - [([L_T] + [P_T] + K_D)^2 - 4[L_T][P_T]]^{1/2}\}/2[L_T] \quad (4)$$

NMR Methods. Phase-sensitive NOESY spectra were obtained at 500 MHz and 15 °C with 50, 75, 100, 125, and 150-ms mixing times by using the method of States et al. (1982). These spectra were collected in arbitrary order during a single 4-day period without removing the sample from the spectrometer or changing the spectrometer settings (Banks et al., 1989). A 180° composite pulse was used during the mixing period to eliminate the contribution of J cross-peaks to the NOE cross-peaks (Macura et al., 1982). The 2D spectra were acquired with 4096 points in t_2, 256 points in t_1, and a spectral width of 6250 Hz in both dimensions. For each t_1 value, 32 scans were collected with a relaxation delay of 2 s. The time domain in t_1 was expanded to 1024 points by zero filling, giving 6-Hz resolution in t_1 and 3-Hz resolution in t_2. The sample used to collect the NOESY spectra contained 0.5 mM RBG200 DHFR, 9 mM $NADP^+$, and 50 mM potassium phosphate buffer, pH* = 5.9,[2] in ^2H_2O. All NMR reagents were chelex-treated before use. Following data collection, the 2D data sets were transferred to a MicroVax II for processing by the FTNMR program (Hare Research Inc.). The NOESY data sets were processed by using a 45° phase-shifted sine bell in t_2 and a Kaiser window in t_1 to avoid truncation effects (Hamming, 1983). The first t_1 value was multiplied by 0.5 to attenuate t_1 ridges in the spectra (Otting et al., 1986). The use of these window functions was shown not to alter the relative magnitude of the NOE cross-peaks. Intensities of the cross-peaks were estimated by measuring volume integrals with FTNMR (Banks et al., 1989; Nerdal et al., 1989). FTNMR sums all points within the operator-specified square footprint.

The time dependence of the NOE buildup curves was used to separate primary NOEs from secondary or spin diffusion effects (Rosevear & Mildvan, 1989). Secondary or spin diffusion effects arising from the indirect transfer of magnetization exhibit a lag in their time-dependent NOE buildup. NOEs resulting from such effects cannot be used directly to determine internuclear distances. Primary NOEs, as judged from the time dependence of the NOE buildup, were used to estimate internuclear distances. The initial slopes of the time-dependent NOE buildup were determined from the linear coefficient of a second-order polynomial fit to the experimental NOE intensities (Hyberts & Wagner, 1989; Baleja et al., 1990). All experimental NOE intensities were utilized in the calculation up to and including the maximum cross-peak intensity for any internuclear pair (Hyberts & Wagner, 1989). Distances were estimated by using eq 5, where R_{ref} and R_{ij}

$$R_{ref}/R_{ij} = r_{ij}^6/r_{ref}^6 \quad (5)$$

are the initial slopes, determined from the time dependence of the NOE, of the known (r_{ref}) and unknown (r_{ij}) interproton distances, respectively. The fixed nicotinamide HN4 to HN5 distance, 2.48 Å, and the fixed ribose H1′ to ribose H2′ distance, 2.9 ± 0.2 Å (Rosevear & Mildvan, 1989), were used as reference distances to estimate unknown distances, r_{ij}, in the NMN and AMN portions of $NADP^+$, respectively. The use of eq 5 assumes isotropic rotation of the molecule as a whole and makes the assumption that all internuclear vectors in either the NMN or AMN portion of $NADP^+$ have the same correlation time (Rosevear & Mildvan, 1989).

Distance Geometry. Internuclear distances, estimated from the time dependence of the NOE, were used in defining upper and lower bound distance constraints in distance geometry calculations to determine the conformations of the NMN and AMN moieties of $NADP^+$ bound to RBG200 DHFR (Kuntz et al., 1979; Havel et al., 1983; Rosevear & Mildvan, 1989). Interproton pairs yielding an estimated distance, using eq 5, of <3.6 Å were given an upper bound distance constraint of <3.6 Å. Pairs of protons giving internuclear distances of >3.6 Å were given lower bound distance constraints of >3.6 Å and upper bound distance constraints of <5.0 Å. Upper and lower bound distance constraints were used, in lieu of absolute distances, to minimize errors introduced into the distances from inaccuracies in measurement of initial NOE buildup rates and estimation of correlation times. Since no NOEs were observed between the NMN and AMN moieties of $NADP^+$, we modeled the bound conformations of the NMN and AMN moieites of $NADP^+$ separately. In the conformational search procedure, each atom of either the NMN or AMN moiety is represented by a point at a known distance from the other atoms. If the distance between any two nonbonded atoms is unknown, the lower bounds are set to the sum of the van der Waals radii, and the upper bounds set at 50 Å to permit the conformation of the molecule to vary freely. Bond lengths and bond angles, expressed as 1–2 and 1–3 distances, respectively, were allowed to vary by 0.01 Å and 0.1 Å. All dihedral angles were expressed as 1–4 distances and allowed to vary by 1.8 Å to permit a complete conformational search. The planarity of the nicotinamide and adenine ring was maintained by using a subroutine that minimizes the weighted sum of the squares of the distances through the atoms of the ring (Rosevear et al., 1983).

[2] pH* denotes a pH meter reading uncorrected for the isotope effect on the equilibrium and on the glass electrode.

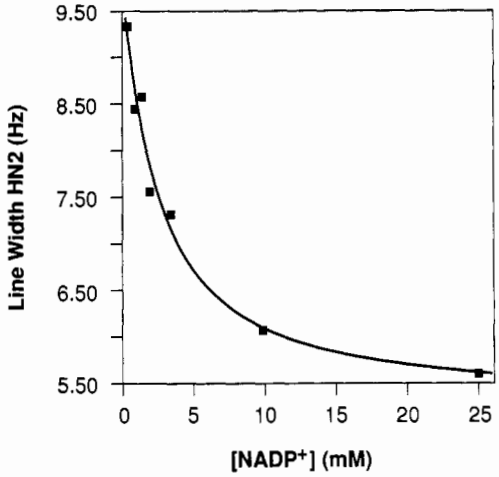

FIGURE 2: Titration measuring the concentration dependence of the line width of the nicotinamide HN2 resonance of $NADP^+$ in the presence of RBG200 DHFR. The sample contained 0.4 mM RBG200 DHFR in the presence of 50 mM potassium phosphate at pH = 5.9 and 25 °C. The curve is a nonlinear least-squares computer fit to the data using eqs 2 and 4 with three variables. The best fit was obtained with a $K_D = 1.9 \pm 0.4$ mM.

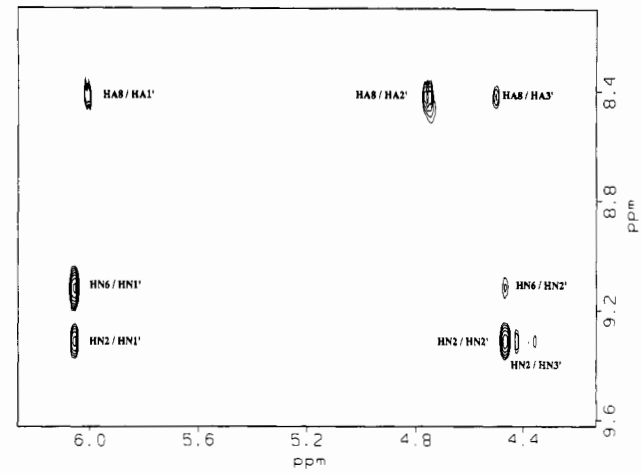

FIGURE 3: Contour plot of the 500-MHz phase-sensitive NOESY spectrum of $NADP^+$ in the presence of RBG200 DHFR in the binary conformation II at 15 °C. The sample contained 0.5 mM RBG200 DHFR and 9 mM $NADP^+$ in 50 mM potassium phosphate buffer in ^2H_2O, pH* = 5.9. The spectrum was recorded with a 100-ms mixing time. Chemical shifts are referenced to external DSS. The labels indicate the assignments of the NOE cross-peaks.

The correct chirality of the asymmetric atoms was maintained by addition of a penalty term based on quantitative deviations from the chiral volume (Rosevear et al., 1983). All internuclear distance constraints, in the form of upper and lower distance bounds, were subjected to a smoothing procedure based on triangle inequalities (Crippen, 1981). Random distances between the upper and lower bounds are chosen and an embedding procedure is utilized to reduce the problem from distance space to three-dimensional space. The embedded structures are then refined by using steepest descent and conjugate gradient minimization. Conjugate gradient minimization is continued until the distance violations in the embedded structures are reduced to the associated input errors. Usually, less than 500 iterations were required to reach suitable low error structures. The fit of each computed structure to the input data is expressed quantitatively by a score that measures the fourth power of the total deviations of the computed and input distances, <1 Å^4. This low error deviation was consistent with no distance violations greater than 1% in the refined structures, planarity of the aromatic rings, and the correct chirality of asymmetric carbons. To effectively search the conformational space consistent with the stereochemical and experimental restraints, 400 structures were calculated. No attempt was made to further refine the calculated structures since enzymes do not necessarily bind low-energy substrate conformations (Mildvan, 1981; Fersht, 1987). The glycosidic torsional angles of the NMN and AMN portions of the computed structures were then evaluated (Saenger, 1984).

Results

Coenzyme Binding Studies to Conformation II. NMR studies monitoring proton chemical shifts of $NADP^+$ upon addition of RBG200 DHFR have permitted the detection of two distinct binary RBG200 DHFR·$NADP^+$ complexes in solution (Brito et al., 1990). Addition of $NADP^+$ to RBG200 DHFR resulted in formation of an initial binary complex (conformation I), which was found to slowly interconvert to a second, more stable, binary complex (conformation II). The binding of oxidized coenzyme to conformation II was studied by equilibrium dialysis at pH = 5.9 using [4-^{3}H]$NADP^+$ and by ^{1}H NMR spectroscopy. From the equilibrium dialysis studies, the binding of $NADP^+$ to RBG200 DHFR in conformation II was found to be weak, $K_D = 1.5 \pm 0.4$ mM. The binding of $NADP^+$ in conformation II was also monitored by measuring the concentration-dependent broadening of the nicotinamide HN2 resonance in the presence of RBG200 DHFR (Figure 2). The change in line width as a function of coenzyme concentration was used to calculate the dissociation constant, K_D, for $NADP^+$ binding to RBG200 DHFR. Nonlinear least-squares analysis yielded a $K_D = 1.9 \pm 0.4$ mM (Figure 2), in good agreement with equilibrium dialysis.

Conformation of $NADP^+$ Bound to RBG200 DHFR. The theory for investigating the structure of enzyme-bound ligands by using TNOEs has been developed (Clore & Gronenborn, 1982, 1983) and the methodology used to determine the conformation of a number of enzyme-bound flexible ligands (Rosevear & Mildvan, 1989; Levy et al., 1983; Ehrlich & Colman, 1985). The conformation of $NADP^+$ bound to RBG200 DHFR was investigated by measuring the time dependence of the transferred NOE in two-dimensional phase-sensitive NOESY spectra. Figure 3 shows an expansion of the contour plot from a 100-ms NOESY spectrum of 9 mM $NADP^+$ in the presence of 0.5 mM RBG200 DHFR at 15 °C, demonstrating selective NOEs between the ribose protons and the nicotinamide and adenine base protons. Assignments of the $NADP^+$ resonances in the presence of RBG200 DHFR were obtained from DQCOSY spectra and are consistent with the known chemical shifts for $NADP^+$ (Oppenheimer, 1982). Large negative internuclear NOEs were observed between the HN2/HN1′, HN2/HN2′, and HN6/HN1′ proton pairs in the NMN portion of $NADP^+$ (Figure 3). Smaller NOEs were also observed between the NH6/HN2′ and HN2/HN3′ proton pairs (Figure 3). In the adenosine moiety, a large NOE was observed between the HA8/HA2′ proton pair, with smaller NOEs between the HA8/HA1′ and HA8/HA3′ proton pairs (Figure 3). Under identical conditions, in the absence of RBG200 DHFR, negative NOEs were not observed up to 500-ms mixing times. Thus, the observed NOEs in the presence of RBG200 DHFR arise from cross-relaxation between protons of $NADP^+$ in the enzyme-bound state and can be used to evaluate the bound conformation of the coenzyme.

The time dependence of the NOE was measured to separate primary NOEs from secondary or spin diffusion effects (Figure 4). Secondary or spin diffusion effects are characterized by a longer lag in the development of the NOE buildup curve than

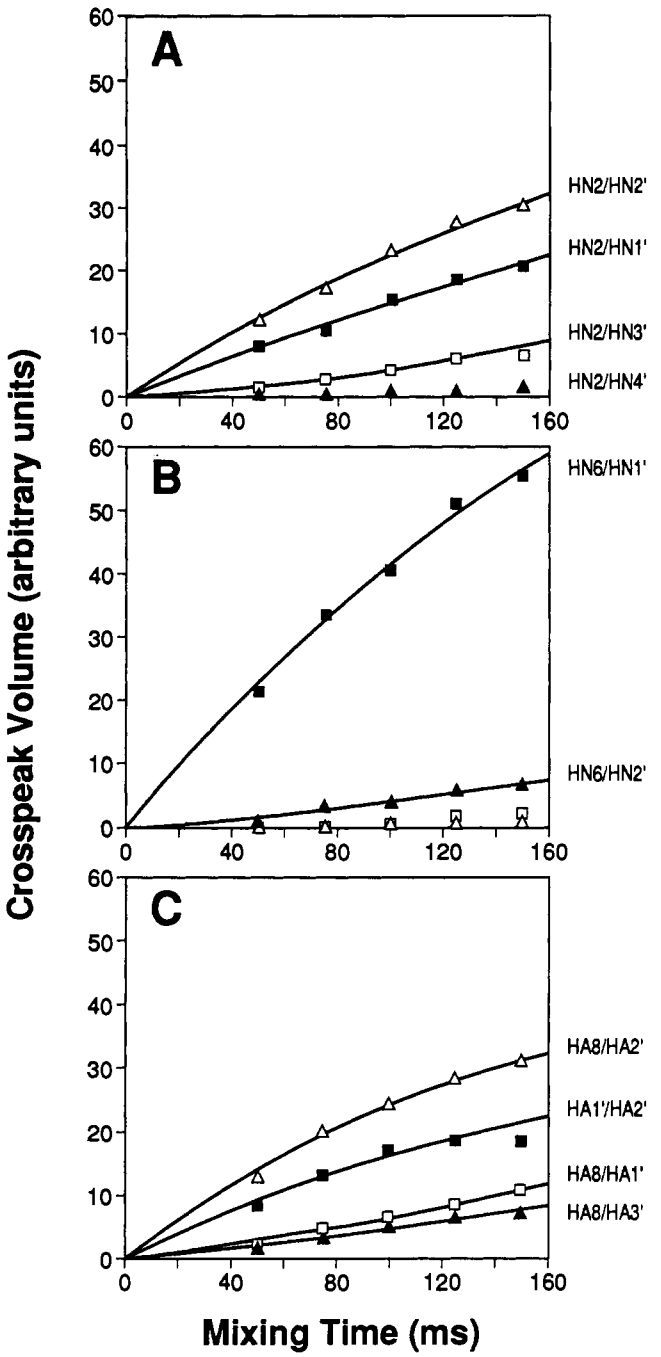

FIGURE 4: Plots of the NOESY cross-peak intensities as a function of the mixing time at 15 °C. (A) NOE buildup curves are shown for HN2/HN1′ (■), HN2/HN2′ (△), HN2/HN3′ (□), and HN2/HN4′ (▲) proton pairs. (B) NOE buildup curves are shown for HN6/HN1′ (■), HN6/HN2′ (▲), HN6/HN3′ (□), and HN6/HN4′ (△) proton pairs. (C) NOE buildup curves are shown for HA1′/HA2′ (■), HA8/HA1′ (□), HA8/HA2′ (△), and HA8/HA3′ (▲) proton pairs. The curves are second-order polynomial fits to the experimental data. Experimental conditions are given in Figure 3.

observed for primary effects, resulting from the time required to transfer magnetization via intermediate spins (Rosevear & Mildvan, 1989). From the time dependence of the NOE buildup curve, primary NOEs were observed between the HN2/HN1′, HN2/HN2′, and HN2/HN3′ proton pairs (Figure 4A). No significant NOE was observed between the HN2/HN4′ proton pair. Figure 4B shows the time-dependent NOE buildup curves for NOEs involving the nicotinamide HN6 proton. A large primary NOE was observed between HN6 and HN1′ (Figure 4B). A small primary NOE was also

Table I: Estimated Distances and Upper and Lower Bound Constraints Derived from the NOE Buildup Rates for NADP+ Bound to RGB200 DHFR in Binary Complex II

spin pair (AB)	r_{AB} (Å)[a]	lower bound (Å)	upper bound (Å)
HN2/HN1′	3.0	vdw[b]	<3.6
HN2/HN2′	2.7	vdw	<3.6
HN2/HN3′	4.7	>3.6	<5.0
HN6/HN1′	2.5	vdw	<3.6
HN6/HN2′	3.9	>3.6	<5.0
HN1′/HN4′	4.2	>3.6	<5.0
HA8/HA1′	3.7	>3.6	<5.0
HA8/HA2′	2.7	vdw	<3.6
HA8/HA3′	3.8	>3.6	<5.0

[a] Internuclear distances within the NMN portion of enzyme-bound NADP+ were estimated by using the initial slope of the HN4/HN5 proton pair and the known HN4/HN5 distance (2.48 Å). Internuclear distances within the AMN portion of enzyme-bound NADP+ were estimated by using the initial slope of the HA1′/HA2′ proton pair and the known HA1′/HA2′ distance (2.9 ± 0.2 Å). [b] Lower limit distance set at the sum of the van der Waals radii of the two atoms.

observed between HN6 and HN2′. The NOEs between the HN6/HN3′ and HN6/HN4′ proton pairs were judged to be secondary due to the lag in the NOE buildup curve (Figure 4B). Primary NOEs were also observed between the HN4/HN5 and HN5/HN6 proton pairs as expected, since the distance between these proton pairs is fixed at 2.48 Å (Clore & Gronenborn, 1983). This pattern of primary NOEs is only consistent with a syn conformation about the nicotinamide–ribose glycosidic bond for enzyme-bound NADP+ (Figures 1 and 4A,B).

Primary NOEs, as judged from the time dependence of the NOE buildup curves, were also observed between the HA8/HA1′, HA8/HA2′, HA8,HA3′, and HA1′/HA2′ proton pairs (Figure 4C). The large primary NOE between the HA8/HA2′ proton pair and the smaller primary NOEs between HA8/HA1′ and HA8/HA3′ proton pairs confine the adenine–ribose glycosidic torsional angle of the AMN moiety of the enzyme-bound NADP+ to an anti conformation.

The lack of internuclear NOEs between the adenine and nicotinamide bases of enzyme-bound NADP+ suggests that NADP+ is bound in an open conformation with the adenine and nicotinamide rings separated by at least 5.0 Å. Previously, a NOE between the HA2 proton and the HN2 or HN6 protons was used to demonstrate that NADPH exists in a folded conformation when bound to isocitrate dehydrogenase (Ehrlich & Colman, 1985).

Initial slopes of the primary NOEs were calculated from the linear coefficient of a second-order polynomial fit to the experimental NOE intensities as described under Methods (Hyberts & Wagner, 1989; Baleja et al., 1990). Internuclear distances (Table I), within the NMN and AMN moieties of enzyme-bound NADP+, were estimated from the initial slopes by using the fixed nicotinamide HN4 to HN5 distance, 2.48 Å, and the fixed ribose H1′ to ribose H2′ distance, 2.9 ± 0.2 Å, as reference distances in eq 5 for the NMN and AMN portions of NADP+, respectively. Hand-built models of the NMN and AMN portions of NADP+ based on the values of the measured distances (Table I) were consistent with syn and anti conformations about the nicotinamide–ribose and adenine–ribose torsional angles of NMN and AMN, respectively. In a more general and objective approach, the experimentally measured internuclear distances (Table I) were used to set upper and lower bound constraints in a distance geometry algorithm to objectively determine the conformations of the NMN and AMN moieties of NADP+ bound to RBG200 DHFR. This approach permits the conformational space of

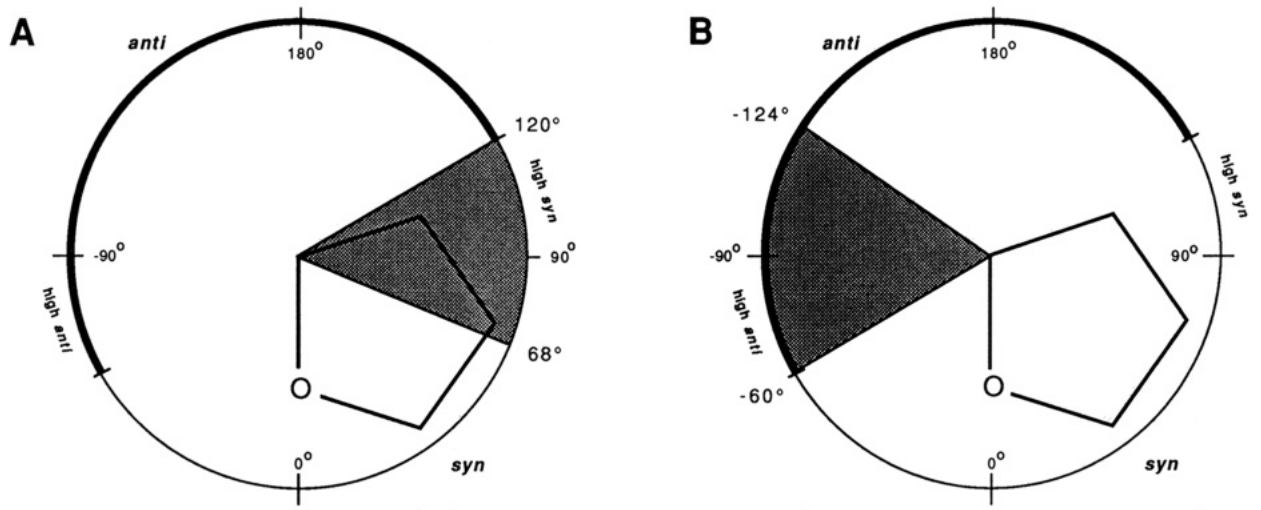

FIGURE 5: Glycosidic torsion angle wheels for the NMN and AMN portions of NADP+ bound to RBG200 DHFR in binary conformation II. (A) The conformational space, defined by the upper and lower bound constraints (Table I), available to the NMN portion of NADP+. (B) The conformational space, defined by the upper and lower bound constraints (Table I), available to the AMN portion of NADP+.

the NMN and AMN portion of NADP+, defined by the experimental distance constraints, to be evaluated. Proton pairs yielding estimated distances of <3.6 Å were given upper bound constraints of 3.6 Å and lower bound constraints equal to the sum of their van der Waals radii (Table I). Proton pairs yielding estimated distances greater than 3.6 Å but less than 5 Å were given an upper bound constraint of 5.0 Å and a lower bound constraint of 3.6 Å (Table I). From these constraints, 400 computer-generated structures were obtained for the NMN and AMN portions of NADP+, respectively. All acceptable structures were found to have internuclear distances that did not deviate by more than 1% from the input bond lengths, bond angles, van der Waals values, and experimental distance constraints. No attempt was made to further refine these structures. With these criteria, all acceptable NMN structures were found to have syn nicotinamide–ribose glycosidic torsional angles ($\chi = 94 \pm 26°$; Figure 5A). Use of the estimated internuclear distances, with a ± 0.4-Å error (Table I), as constraints in the distance geometry calculation did not significantly alter the average or the range of acceptable nicotinamide–ribose glycosidic torsional angles. These results demonstrate that qualitative interpretation of the observed NOEs in combination with distance geometry calculations is sufficient to evaluate the range of conformations available to the NMN moiety of NADP+ bound to RBG200 DHFR. For AMN, all of the acceptable solutions were found to have anti adenine–ribose glycosidic torsional angles ($\chi = -92 \pm 32°$; Figure 5B). Thus, in the second binary NADP+·RBG200 DHFR complex, the oxidized coenzyme is bound with a syn conformation about the nicotinamide–ribose and an anti conformation about the adenine–ribose glycosidic bonds (Figure 5).

Qualitative Comparison of Enzyme-Bound NADP+ in Binary Conformations I and II. In order to qualitatively compare the enzyme-bound conformations of NADP+ in both binary complexes I and II, NOESY spectra were collected at 5 °C. Under these conditions, at the end of the experiment approximately 25% of the initial binary complex, conformation I, had converted to conformation II (Brito et al., 1990). Figure 6 shows an expanded region of the 150-ms NOESY at 5 °C of NADP+ bound to RBG200 DHFR in conformations I and II. In conformation I, large NOE cross-peaks were observed between the HN6/HN1′ and the HN2/HN2′ proton pairs (Figure 6A). Smaller NOE cross-peaks were observed between the HN2/HN1′ and the HN2/HN3′ proton pairs. This

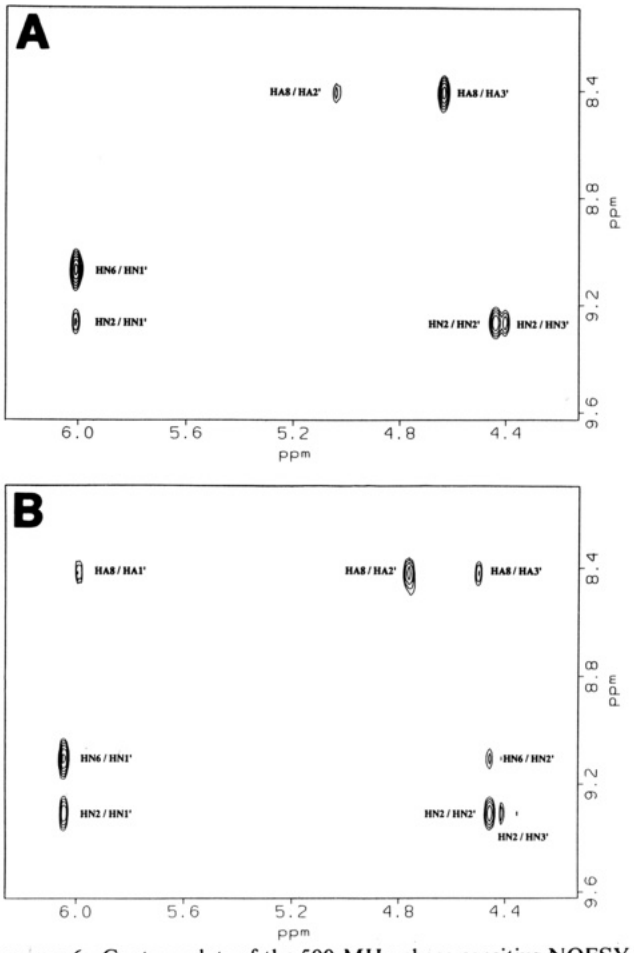

FIGURE 6: Contour plots of the 500-MHz phase-sensitive NOESY spectra of NADP+ bound to RBG200 DHFR in the binary complexes I and II at 5 °C. (A) Expanded region of the 150-ms NOESY spectrum showing the NOE cross-peak intensities for enzyme-bound NADP+ in binary conformation I. (B) Expanded region of the 150-ms NOESY spectrum showing the NOE cross-peak intensities for enzyme-bound NADP+ in binary conformation II. Experimental conditions are given in Figure 3.

pattern of NOEs qualitatively confines the glycosidic torsional angle about the nicotinamide–ribose bond to a syn conformation for NADP+ bound in conformation I (Figure 1). In conformation I, a large NOE was also observed between the HA8/HA3′ proton pair and a smaller NOE observed between

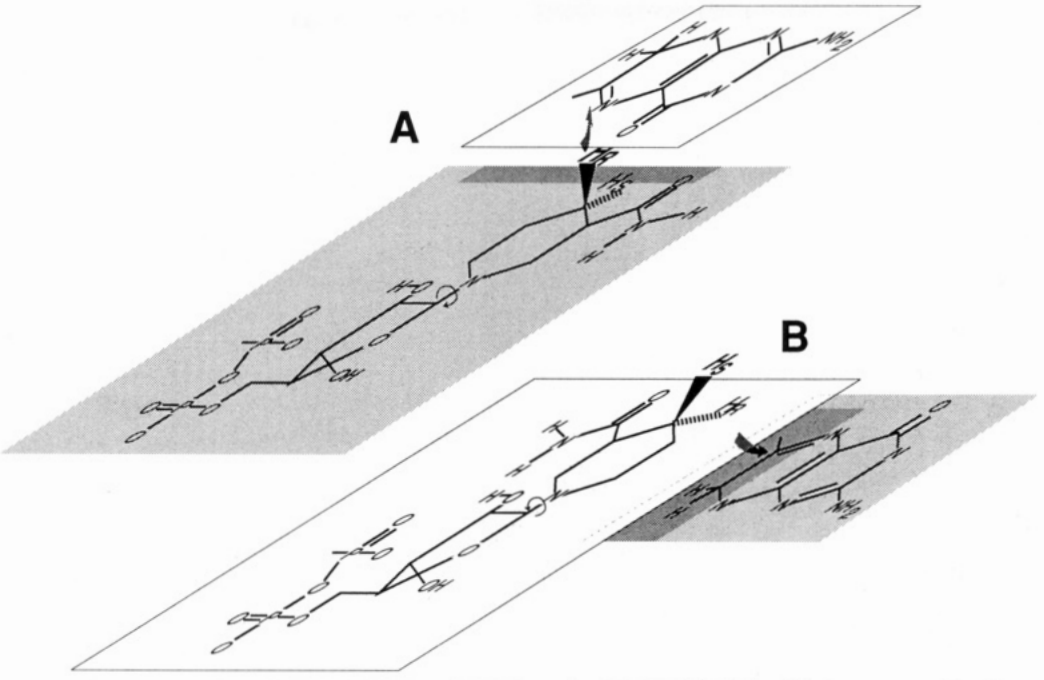

FIGURE 7: Comparison of the proposed model for NADPH and DHF bound to RBG200 DHFR with that proposed for *L. casei* DHFR. (A) Spatial relationship between NADPH and the pteridine ring of DHF in the binding site of *L. casei* DHFR as modeled by Filman et al., (1982) based on the crystal structure of the *L. casei* DHFR·NADPH·methotrexate ternary complex. The NMN portion of NADPH is bound in the anti conformation and the nicotinamide ring is located in a plane below the plane of the pteridine ring of DHF. (B) Proposed model of the spatial relation between NADPH and the pteridine ring of DHF in the binding site of RBG200 DHFR. The NMN portion of NADPH is bound in the syn conformation and the nicotinamide ring is located in a plane above the plane of the pteridine ring, permitting the *pro-R* hydrogen of NADPH to be transferred to the pteridine.

the HA8/HA2′ proton pair (Figure 6A). These NOEs qualitatively constrain the glycosidic torsional angle about the adenine–ribose bond to an anti conformation for NADP+ bound in conformation I.

After complete interconversion of conformation I to II, as determined by the chemical shifts of NADP+ (Brito et al., 1990), a second NOESY spectrum was obtained under identical conditions. A similar pattern of NOE cross-peak intensities was observed at 5 °C for NADP+ bound to RBG200 DHFR in conformation II (Figure 6B). However, intensity ratios between identical NOEs were found to vary (Figure 6). The NOE cross-peak intensity ratio between the HN6/HN1′ and the HN2/HN1′ proton pairs was found to be closer to unity than observed in conformation I (Figure 6). Additionally, a small NOE was observed between the HN6/HN2′ proton pairs (Figure 6B). This pattern of NOE cross-peak intensities was found to be identical with that observed at 15 °C for NADP+ binding to RBG200 DHFR in conformation II (Figure 3). The pattern of interproton NOEs observed in the NMN portion of NADP+ bound to RBG200 DHFR in conformation II at 5 °C (Figure 6B) confines the nicotinamide–ribose glycosidic torsional angle to a syn conformation, as was previously observed at 15 °C (Figure 3). Within the AMN moiety of NADP+ bound in conformation II, the large NOE cross-peak between the HA8/HA2′ proton pair and the smaller NOE cross-peaks between the HA8/HA3′ and the HA8/HA1′ proton pairs qualitatively define the adenine–ribose glycosidic torsional angle to an anti conformation (Figure 1). However, several interesting features appear when cross-peak intensities within the AMN moiety of NADP+ bound to RBG200 DHFR in conformations I and II are compared (Figure 6). In conformation II, the ratio of interproton NOE cross-peaks in the AMN moiety was found to be HA8/HA2′ $\gg$ HA8/HA3′ $\approx$ HA8/HA1′ (Figure 6B); however, in conformation I the ratio of interproton NOE cross-peaks was found to be HA8/HA3′ $\gg$ HA8/HA2′ (Figure 6A). Thus, conversion of binary conformation I to II appears to alter the adenine–ribose glycosidic torsional angle.

Discussion

Dehydrogenases are known to catalyze the stereospecific transfer of hydrogen between their coenzyme, NADH or NADPH, and substrate. These enzymes can be grouped into two classes: A stereospecific, which transfer the C4 *pro-R* hydrogen, and B stereospecific, which transfer the C4 *pro-S* hydrogen of the reduced nicotinamide ring (You, 1985). As a general rule, dehydrogenases transferring the *pro-R* hydrogen have been shown to bind the coenzyme with an anti conformation about the nicotinamide–ribose glycosidic bond. In contrast, enzymes transferring the *pro-S* hydrogen have been shown to bind the coenzyme with a syn conformation about the nicotinamide–ribose bond (Benner, 1982; Levy et al., 1983; You, 1985). As pointed out by Oppenheimer (1986), this makes the assumption that the substrate binds on top of the coenzyme. If the coenzyme binds on top of the substrate, the opposite correlation would apply. An example of this is glutathione reductase, which is known to transfer the *pro-S* hydrogen of NADPH, but to bind NADPH with an anti conformation about the nicotinamide–ribose glycosidic bond (Pai & Schulz, 1983). Examination of the crystallographic structure shows that NADPH is stacked on top of the flavin part of the bound FAD (Pai & Schulz, 1983).

Chromosomal dihydrofolate reductases are known to transfer the *pro-R* hydrogen from NADPH to dihydrofolate and to bind NADPH with an anti conformation about both the nicotinamide–ribose and adenine–ribose glycosidic bonds (Charlton et al., 1979; You, 1982; Matthews et al., 1979). For example, the NMN moiety of NADPH bound to chromosomal *Lactobacillus casei* DHFR has been shown by crystallography to have an anti glycosidic torsional angle, $\chi = -141°$ (Matthews et al., 1979). The schematic arrangement of substrates at the active site of *L. casei* DHFR based on the stereochem-

istry of hydride transfer and the enzyme-bound conformation of NADPH is shown in Figure 7A (Bolin et al., 1982). Dihydrofolate is located above the plane of the nicotinamide ring, such that the *pro-R* hydrogen can be transferred to C6 of the pteridine ring of DHF (Figure 7A).

Type II DHFRs encoded by the R67 and R388 plasmids are structurally different from the chromosomal DHFRs and relatively insensitive to antifolate compounds such as trimethoprim and methotrexate (Pattishall et al., 1977). The crystal structure of a dimeric form of R67 DHFR in the absence of cofactor and substrate was found to be a dimer of two identical subunits each folded into a β-barrel conformation (Matthews et al., 1986). On the basis of modeling studies using the R67 dimer, the substrate and cofactor were proposed to bind in a "gap" along one face of the antiparallel β-barrel. In contrast, the cofactor binding domain at the active site of chromosomal DHFRs structurally resembles the cofactor binding domains in other NAD^+-dependent dehydrogenases (Kraut & Matthews, 1986). Modeling studies, assuming that type II DHFR transferred the *pro-R* hydrogen of the reduced nicotinamide, also suggested that NADPH was bound with an anti conformation about both the nicotinamide–ribose and adenine–ribose glycosidic bonds (Matthews et al., 1986). Attempts to construct a model with a syn conformation about the nicotinamide–ribose glycosidic bond of $NADP^+$ were unsuccessful (Matthews et al., 1986).

Type II DHFRs have been found to be tetramers composed of four identical subunits (Smith et al., 1979; Brito et al., 1990). RBG200 DHFR was shown to stereospecifically transfer the *pro-R* hydrogen of NADPH to the C6 *si* face of the pteridine ring in dihydrofolate, making it a member of the A-stereospecific class of dehydrogenases (Brito et al., 1990). Thus, although RBG200 DHFR is sequentially and structurally different from known chromosomal DHFRs, both enzymes catalyze identical hydrogen-transfer reactions. NMR studies have detected the existence of two distinct binary $NADP^+$·RBG200 DHFR complexes. Addition of $NADP^+$ to RBG200 DHFR results in formation of an initial binary complex, conformation I, which slowly interconverts to a second more stable complex, conformation II (Brito et al., 1990).

As a consequence of the proposed novel mode of cofactor binding by type II DHFRs, we initiated structural studies on RBG200 DHFR to determine the conformation of $NADP^+$ bound to RBG200 DHFR in both conformations I and II. The combination of internuclear distances, estimated from the initial slope of NOE buildup curves, Table I, and distance geometry calculations was used to define the conformational space available to the nicotinamide–ribose and adenine–ribose glycosidic torsional angles of $NADP^+$ bound to RBG200 DHFR in conformation II. Unexpectedly, the average nicotinamide–ribose glycosidic torsional angle for enzyme-bound $NADP^+$ was found to be syn, $\chi = 94 \pm 26°$, for all acceptable solutions (Figure 5A). The internuclear distances estimated for the NMN portion of enzyme-bound $NADP^+$ were consistent with a unique conformation for the coenzyme. However, the wide range of acceptable syn conformations suggests that the NMN portion of enzyme-bound $NADP^+$ may have considerable mobility within this range of syn conformations. Multiple nicotinamide–ribose conformations, syn and anti, for $NADP^+$ at the active site of RBG200 DHFR cannot unequivocally be ruled out by use of a single technique (Rosevear et al., 1983), although NOEs have previously been used to demonstrate multiple conformations for enzyme-bound nucleotides (Rosevear et al., 1987). In addition, the small initial buildup rate of the HN6/HN2′ NOE rules out the presence of a significant population of enzyme-bound $NADP^+$ having an anti conformation about the nicotinamide–ribose bond (Levy et al., 1983). Our data are self-consistent only with a syn conformation about the nicotinamide–ribose glycosidic bond in the binary complex.

Based on the observed stereochemistry of hydride transfer and the enzyme-bound conformation of the NMN portion of $NADP^+$, a hypothetical model for the arrangement of cofactor and DHF at the active site of RBG200 DHFR is shown in Figure 7B. In this model, the nicotinamide–ribose glycosidic torsional angle of NADPH is syn with the *pro-R* hydrogen below the plane of the nicotinamide ring. For this hydrogen to be transferred to the C6 *si* face of the pteridine ring in DHF, the pteridine portion of DHF must be below the plane of the nicotinamide ring, and rotated 180° with respect to DHF binding in chromosomal DHFRs (Figure 7). With the arrangement of substrates proposed in Figure 7B, type II DHFRs obey the correlation observed between the nicotinamide–ribose torsional angle and hydride-transfer stereochemistry. This arrangement of substrates in the active site of RBG200 DHFR may explain the weaker binding of 2,4-diamino heterocycles to type II DHFRs, since the location of hydrogen bonding donors and acceptors at the pteridine binding site on type II DHFRs must be different from that found in chromosomal enzymes. Although unlikely, the possibility cannot be ruled out that the conformation of the bound cofactor is significantly different, syn versus anti about the nicotinamide–ribose glycosidic linkage, in the presence of substrate.

The enzyme-bound conformation of the AMN portion of $NADP^+$ in conformation II was also investigated by using the estimated internuclear distances (Table I) and distance geometry calculations. Upper and lower bound constraints, obtained from the estimated internuclear distances, were sufficient to define the adenine–ribose glycosidic torsional angle, $\chi = -92 \pm 32$ (Figure 5B). The anti glycosidic torsional angle about the adenine–ribose bond is consistent with that found for NADPH bound to chromosomal DHFRs (Matthews et al., 1979) and other NAD(P) binding proteins (Levy et al., 1983; Ehrich & Colman, 1985).

The lack of observed internuclear NOEs between the adenine and nicotinamide bases suggests that $NADP^+$ is not bound to RBG200 DHFR in a stacked or folded conformation and that the distance between the two aromatic rings in the bound coenzyme must be at least 5 Å. Overhauser effects between the two nucleotide rings have previously been used to demonstrate that NADPH exists in a stacked or folded conformation when bound to isocitrate dehydrogenase (Ehrlich & Colman, 1985). Folded conformations of the coenzyme have also been observed for NADH bound to the allosteric effector site and the nucleoside inhibitor site of phosphorylase *b* (Stura et al., 1983).

The conformation of $NADP^+$ bound to RBG200 DHFR in the initial binary complex, conformation I, was qualitatively evaluated at 5 °C, to decrease the interconversion rate between conformation I and II. The pattern of internuclear NOEs, Figure 6A, was only consistent with syn and anti conformations about the nicotinamide–ribose and adenine–ribose glycosidic bonds for the NMN and AMN portions of $NADP^+$ bound to RBG200 DHFR in conformation I. The pattern of internuclear NOEs at 5 °C, after conversion to conformation II, was qualitatively similar to that obtained at 15 °C (Figures 3 and 6B). Thus, the nicotinamide–ribose and the adenine–ribose glycosidic torsional angles of the NMN and AMN moieties of enzyme-bound $NADP^+$ were found to be syn and anti,

respectively, in both binary conformations. However, from the magnitude of the NOE cross-peak intensities, minor conformational differences were detected between the enzyme-bound conformations of NADP+ in the two distinct binary complexes.

In conclusion, the stereochemistry of hydride transfer and the enzyme-bound conformation of NADP+ have permitted us to propose an unique arrangement of coenzyme and DHF at the active site of a type II DHFR (Figure 7B). This novel arrangement of substrates, compared to chromosomal DHFRs, may be responsible for the resistance of this class of DHFRs to the antifolate compounds. Studies are currently in progress to determine the enzyme-bound conformation of the cofactor in ternary complexes with DHF, trimethoprim, and methotrexate. These studies, along with identification of the amino acids involved in substrate binding and catalysis, will permit us to refine the proposed model for cofactor binding and to better understand the resistance of type II DHFRs to antifolate compounds.

References

Amyes, S. G. B., & Smith, J. T. (1974) *Biochem. Biophys. Res. Commun. 58*, 412.

Aymes, S. G. B. & Smith, J. T. (1976) *Eur. J. Biochem. 61*, 597.

Balcja, J. D., Moult, J., & Sykes, B. D. (1990) *J. Magn. Reson. 87*, 375.

Banks, K. M., Hare, D. R., & Reid, B. R. (1989) *Biochemistry 28*, 6996.

Benner, S. A. (1982) *Experientia 38*, 633.

Bolin, J. T., Filman, D. J., Matthews, D. A., Hamlin, R. C., & Kraut, J. (1982) *J. Biol. Chem. 257*, 13650.

Brito, R. M. M., Reddick, R., Bennett, G. N., Rudolph, F. B., & Rosevear, P. R. (1990) *Biochemistry 29*, 9825.

Campbell, I. D., & Dwek, R. A. (1984) in *Biological Spectroscopy*, The Benjamin/Cummings Publishing Company, Inc., London.

Charlton, P. A., Young, D. W., Birdsall, B., Feeney, J., & Roberts, G. C. K. (1979) *J. Chem. Soc., Chem. Commun.*, 922.

Clore, G. M., & Gronenborn, A. M. (1983) *J. Magn. Reson. 48*, 402.

Clore, G. M., & Gronenborn, A. M. (1982) *J. Magn. Reson. 53*, 423.

Crippen, G. M. (1981) *Distance Geometry and Conformational Calculations* (Bawden, D., Ed.) Research Studies Press, Chichester, England.

Ehrlich, R. S., & Colman, R. F. (1985) *Biochemistry 24*, 5378.

Feeney, J., Birdsall, B., Roberts, G. C. K., & Burgen, A. S. V. (1983) *Biochemistry 22*, 628.

Fersht, A. R. (1987) *Biochemistry 26*, 8031.

Filman, D. J., Bolin, J. T., Matthews, D. A., & Kraut, J. (1982) *J. Biol. Chem. 257*, 13663.

Fleming, M. P., Datta, N., & Grüneburg, R. N. (1972) *Br. Med. J. 1*, 726.

Hamming, R. W. (1983) in *Digital Filters*, 2nd ed., Princeton Hall, NJ.

Hitchings, G. H., & Smith, S. L. (1980) *Adv. Enzyme Regul. 18*, 349.

Hyberts, S. G., & Wagner, G. (1989) *J. Magn. Reson. 81*, 418.

Kraut, J., & Matthews, D. A. (1986) in *Biological Macromolecules and Assemblies* (Journak, F., & McPherson, A., Eds.) Vol. III, pp 1–71, Wiley, New York.

Kuntz, I. D., Crippen, G. M., & Kollman, P. A. (1979) *Biopolymers 18*, 939.

Levy, H. R., Ejchart, A., & Levy, G. C. (1983) *Biochemistry 22*, 2792.

Macura, S., Wüthrich, K., & Ernst, R. R. (1982) *J. Magn. Reson. 47*, 351.

Matthews, D. A., Alden, R. A., Freer, S. T., Xuong, N., & Kraut, J. (1979) *J. Biol. Chem. 254*, 4144.

Matthews, D. A., Smith, S. L., Baccarani, D. P., Burchall, J. J., Oatley, S. J., & Kraut, J. (1986) *Biochemistry 26*, 4194.

Mildvan, A. S. (1981) *Philos. Trans. R. Soc. London, B 293*, 65.

Nerdal, W., Hare, D. R., & Reid, B. R. (1989) *Biochemistry 28*, 10008.

Oppenheimer, N. J. (1982) in *The Pyridine Nucleotide Coenzymes* (Everse, J., Anderson, B., & You, K. S., Eds.) pp 51–89, Academic Press, New York.

Oppenheimer, N. J. (1986) *J. Biol. Chem. 261*, 12209.

Otting, G., Widmer, H., Wagner, G., & Wüthrich, K. (1986) *J. Magn. Reson. 66*, 187.

Pai, E. F., & Schulz, G. E. (1983) *J. Biol. Chem. 258*, 1752.

Pattishall, K. H., Acar, J., Burchall, J. J., Goldstein, F. W., & Harvey, R. J. (1977) *J. Biol. Chem. 252*, 2319.

Rosevear, P. R., & Mildvan, A. S. (1990) *Methods Enzymol. 177*, 333.

Rosevear, P. R., Bramson, H. N., O'Brian, C., Kaiser, E. T., & Mildvan, A. S. (1983) *Biochemistry 22*, 3439.

Rosevear, P. R., Fox, T. L., & Mildvan, A. S. (1987) *Biochemistry 26*, 3487.

Saenger, W. (1984) in *Principles of Nucleic Acid Structure* (Cantor, C. R., Ed.) pp 9–28, Springer-Verlag, New York.

Skold, O., & Widh, A. (1974) *J. Biol. Chem. 249*, 4324.

Smith, S. L., & Burchall, J. J. (1983) *Proc. Natl. Acad. Sci. U.S.A. 80*, 4619.

Smith, S. L., Stone, D., Novak, P., Baccanari, D. P., & Burchall, J. J. (1979) *J. Biol. Chem. 254*, 6222.

States, D. J., Haberkorn, R. A., & Ruben, D. J. (1982) *J. Magn. Reson. 48*, 286.

Stura, E. A., Zanotti, G., Babu, Y. S., Sansom, M. S. P., Stuart, D. I., Wilson, K. S., Johnson, L. N., & Van de Werve, G. (1983) *J. Mol. Biol. 170*, 529.

Vermersch, P. S., Klass, M. R., & Bennett, G. N. (1986) *Gene 41*, 289.

You, K.-S. (1982) *Methods Enzymol. 87*, 101.

You, K.-S. (1985) *Crit. Rev. Biochem. 17*, 313.

Zolg, J. W., & Hänggi, U. J. (1981) *Nucleic Acids Res. 9*, 697.